

The Indian Ocean Experiment: Widespread Air Pollution from South and Southeast Asia

J. Lelieveld,^{1*} P. J. Crutzen,^{1,2} V. Ramanathan,² M. O. Andreae,¹
 C. A. M. Brenninkmeijer,¹ T. Campos,³ G. R. Cass,⁴
 R. R. Dickerson,⁵ H. Fischer,¹ J. A. de Gouw,⁶ A. Hansel,⁷
 A. Jefferson,⁸ D. Kley,⁹ A. T. J. de Laat,⁶ S. Lal,¹⁰
 M. G. Lawrence,¹ J. M. Lobert,² O. L. Mayol-Bracero,¹
 A. P. Mitra,¹¹ T. Novakov,¹² S. J. Oltmans,⁸ K. A. Prather,¹³
 T. Reiner,¹ H. Rodhe,¹⁴ H. A. Scheeren,⁶ D. Sikka,¹⁵ J. Williams¹

The Indian Ocean Experiment (INDOEX) was an international, multiplatform field campaign to measure long-range transport of air pollution from South and Southeast Asia toward the Indian Ocean during the dry monsoon season in January to March 1999. Surprisingly high pollution levels were observed over the entire northern Indian Ocean toward the Intertropical Convergence Zone at about 6°S. We show that agricultural burning and especially biofuel use enhance carbon monoxide concentrations. Fossil fuel combustion and biomass burning cause a high aerosol loading. The growing pollution in this region gives rise to extensive air quality degradation with local, regional, and global implications, including a reduction of the oxidizing power of the atmosphere.

Until recently, North America and Europe dominated the use of fossil fuels, resulting in strong carbon dioxide emissions and global warming (1). The fossil energy-related CO₂ release per capita in Asia is nearly an order of magnitude smaller than in North America and Europe (2). However, Asia is catching up. About half of the world's population lives in South and East Asia, and hence the potential for growing pollutant emissions is large. In China, many pollution sources reduce air quality (3–5). In rural residential areas, notably in India, the burning of biofuels, such as wood, dung, and agricultural waste, is a major source of pollutants (6). In urban areas, the increasing energy demand for industry

and transport propels fossil fuel utilization (7).

Here we evaluate measurements of the Indian Ocean Experiment (INDOEX) to characterize the atmospheric chemical composition of the outflow from South and Southeast Asia, from January to March 1999 during the dry winter monsoon (8). During this season, the northeasterly winds are persistent, and convection over the continental source regions is suppressed by large-scale subsidence, thus limiting upward dispersion of pollution (9). Our analysis is based on measurements from a C-130 and a Citation aircraft operated from the Maldives near 5°N, 73°E, the research vessels *Ronald H. Brown* and *Sagar Kanya*, and the Kaashidhoo Climate Observatory (KCO) on the Maldives (Fig. 1). During the campaign, the location of the Intertropical Convergence Zone (ITCZ) varied between the equator and 12°S. Hence, transport of primary pollutants and reaction products toward the ITCZ could be studied over an extended ocean area where pollutant emissions are otherwise minor. By performing measurements across the ITCZ, the polluted air masses could be contrasted against comparatively clean air over the southern Indian Ocean. Furthermore, we used the measurements to evaluate the numerical representation of these processes in a chemistry general circulation model (GCM) (10). The model was subsequently applied to calculate the large-scale atmospheric chemical effects of the measured pollution.

Aerosol chemical and optical measurements were performed from both aircraft, the R/V *Brown*, and KCO. The latter is located

the CIMS, air was sampled with an inlet specially designed to separate gas- and particle-phase HNO₃ by using a modified virtual impactor technique. During most flights, gas and particle phases were sampled alternately for periods of ~3 min each. The CIMS data confirm the NO_y component of the large particles as HNO₃ on 20 January and provide size and number concentration evidence consistent with the NO_y observations. With the MASP probe, the distribution of particles was measured for sizes from 0.3 to 22 μm in diameter on 20 January. The probe data confirm the presence of many small PSC particles between 0.3 and 2 μm and a few larger particles up to 20 μm in diameter. The probe data for the size and number of the larger particles are nominally consistent with the results in Fig. 4, although the statistical uncertainty is high because of low count rates. The number of particles in the size range of the small simulation mode in Fig. 4 is also nominally consistent with the probe data.

17. No direct measurements of particle shape are available. However, particles composed of solid HNO₃ hydrates are generally assumed to be nonspherical, even at sizes of <5 μm, because of lidar depolarization measurements [e.g., (40)]. Although modest corrections to fall speed and sampling efficiency calculations may ultimately be warranted because of nonspherical shapes, the assumption of sphericity is adopted here throughout for simplicity.
18. D. R. Worsnop, L. E. Fox, M. S. Zahniser, S. C. Wofsy, *Science* **259**, 71 (1993).
19. D. Hanson, K. Mauersberger, *Geophys. Res. Lett.* **15**, 855 (1988).
20. Supplementary material is available at www.sciencemag.org/cgi/content/full/291/5506/1026/DC1.
21. R. Müller, Th. Peter, *Ber. Bunsenges. Phys. Chem.* **96**, 353 (1992).
22. Denitrification is often observed with dehydration. Dehydration is rare in the Arctic vortex, whereas it is expected every winter in the Antarctic (7, 41). In the Arctic 1999/2000 winter, significant dehydration [up to 0.5 parts per million by volume (ppmv)] was observed at flight altitudes once during a brief period on a flight after 20 January.
23. M. Santee et al., *Geophys. Res. Lett.* **27**, 3213 (2000).
24. G. L. Manney, J. L. Sabutis, *Geophys. Res. Lett.* **27**, 2589 (2000).
25. K. S. Carslaw, data not shown.
26. HNO₃ was observed remotely in the 5 to 8 km above the ER-2 aircraft by a microwave radiometer (42). The radiometer flew on board the NASA DC-8 aircraft during SOLVE/THESEO 2000.
27. T. Deshler et al., *J. Atmos. Chem.* **30**, 11 (1998).
28. J. C. Wilson et al., *Geophys. Res. Lett.* **17**, 361 (1990).
29. A. Tabazadeh et al., *Science* **288**, 1407 (2000).
30. T. Koop et al., *Geophys. Res. Lett.* **22**, 917 (1995).
31. U. M. Biermann et al., *Geophys. Res. Lett.* **23**, 1693 (1996).
32. D. Hofmann, *Geophys. Res. Lett.* **17**, 369 (1990).
33. D. M. Murphy, D. S. Thomson, M. J. Mahoney, *Science* **282**, 1664 (1998).
34. S. C. Wofsy et al., *Geophys. Res. Lett.* **17**, 449 (1990).
35. M. L. Santee et al., *Science* **267**, 849 (1995).
36. B.-M. Sinnhuber et al., *Geophys. Res. Lett.* **27**, 3483 (2000).
37. D. T. Shindell, D. Rind, P. Lonergan, *Nature* **392**, 589 (1998).
38. S. J. Oltmans, D. J. Hofmann, *Nature* **374**, 146 (1995).
39. D. Baumgardner et al., *Geophys. Res. Lett.* **23**, 749 (1996).
40. E. V. Browell et al., *Geophys. Res. Lett.* **17**, 385 (1990).
41. K. H. Rosenlof et al., *J. Geophys. Res.* **102**, 13213 (1997).
42. H. Küllman et al., in *Air Pollution Research Report 73*, N. R. P. Harris, M. Guirlet, G. T. Amanatidis, Eds. (European Commission, Brussels, 2000), pp. 699–702.
43. K. K. Kelly, *J. Geophys. Res.* **98**, 8713 (1993).
44. We appreciate the contributions of J. Barrilleaux, J. Nystrom, and D. Porter as NASA ER-2 pilots; of L. Lait in producing Fig. 1; and of B. P. Luo in discussions of the statistical evaluation of the particle size distributions. The NASA Upper Atmosphere Research Program supported this research.

¹Max-Planck-Institute for Chemistry, Post Office Box 3060, D-55020 Mainz, Germany. ²Center for Atmospheric Sciences, Scripps Institution of Oceanography, La Jolla, CA 92093–4922, USA. ³National Center for Atmospheric Research, Boulder, CO 80303, USA. ⁴School of Earth and Atmospheric Sciences, Georgia Institute of Technology, Atlanta, GA 30332–0340, USA. ⁵Department of Meteorology, University of Maryland, College Park, MD 20742, USA. ⁶Utrecht University, 3584 CC Utrecht, Netherlands. ⁷University of Innsbruck, A-6020 Innsbruck, Austria. ⁸Climate Monitoring and Diagnostics Laboratory, National Oceanic and Atmospheric Administration, Boulder, CO 80303, USA. ⁹Research Centre Jülich, ICG-2, D-52428, Jülich, Germany. ¹⁰Physical Research Laboratory, Navrangpura, Ahmedabad 380 009, India. ¹¹National Physical Laboratory, New Delhi 110 012, India. ¹²Lawrence Berkeley National Laboratory, Berkeley, CA 94720, USA. ¹³University of California, Riverside, CA 92521–0403, USA. ¹⁴Department of Meteorology, Stockholm University, S-10691 Stockholm, Sweden. ¹⁵40 Mausam Vihar, New Delhi 110051, India.

*To whom correspondence should be addressed. E-mail: lelieveld@mpch-mainz.mpg.de

REPORTS

on a small island about 500 km southwest of India and more than 1000 km from the main pollution centers. At KCO, we measured the size distribution and chemical composition of fine particles, collected on filters and cascade impactors (11). The filter analysis shows an average dry mass concentration of $\sim 17 \mu\text{g}/\text{m}^3$ (Fig. 2). The aerosol contained substantial amounts of both inorganic and organic pollutants, including black carbon (BC). Mass spectrometric particle analysis shows that the BC particles were always mixed with organics and sulfate, indicating substantial chemical processing. Very similar results were obtained from KCO, the boundary layer flights by the C-130 aircraft, and the R/V *Brown*, which shows that the aerosol composition was remarkably uniform over the northern Indian Ocean.

The aerosol mass loading observed over the Indian Ocean is quite comparable to suburban air pollution in North America and Europe (12). However, the BC content was relatively high (Table 1), which gives the aerosol a strong sunlight-absorbing character, yielding a single scattering albedo at ambient relative humidity between 0.8 and 0.9. This aerosol, with a mean optical depth of 0.2 to

0.4 (at 0.63- μm wavelength), reduces solar heating of the northern Indian Ocean by about 15% ($\sim 25 \text{ W}/\text{m}^2$) and enhances the heating of the boundary layer by about 0.4 K/day ($\sim 12 \text{ W}/\text{m}^2$), which substantially perturbs the regional hydrological cycle and climate (13, 14).

The BC aerosol and fly ash are unquestionably human produced because natural sources are negligible. Likewise, non-sea-salt sulfate can be largely attributed to anthropogenic sources. Filter samples collected on board the R/V *Brown* in the clean marine boundary layer south of the ITCZ reveal a fine aerosol sulfate concentration of about $0.5 \mu\text{g}/\text{m}^3$, probably from the oxidation of naturally emitted dimethyl sulfide. The sulfate concentration over the northern Indian Ocean was close to $7 \mu\text{g}/\text{m}^3$, and we thus infer an anthropogenic fraction of more than 90%. Similarly, the ammonium concentration south of the ITCZ, from natural ocean emissions, was $0.05 \mu\text{g}/\text{m}^3$, indicating an anthropogenic contribution of more than 95% to the nearly $2 \mu\text{g}/\text{m}^3$ of ammonium observed north of the ITCZ.

It is more difficult to attribute the organic aerosol fraction to a particular source category.

Secondary organic particles from natural hydrocarbon sources are probably of minor importance because India is scarcely forested. Moreover, the BC/total carbon ratio of 0.5, as derived from the filter samples, is typical for aerosols from fossil fuel combustion (15). In the aerosol south of the ITCZ, organic compounds were negligible, whereas over the northern Indian Ocean, it was almost $6 \mu\text{g}/\text{m}^3$. We thus infer that most of the particulate organics north of the ITCZ were of anthropogenic origin. INDOEX aerosol components of natural origin included a total mass fraction of 1% sea salt and 10% mineral dust. Nevertheless, some of the mineral aerosol likely originated from road dust and agricultural emissions. Taken together, the human-produced contribution to the aerosol was at least 85%. Because precipitation is scarce during the winter monsoon, the aerosol can spread over the entire northern Indian Ocean before entering the ITCZ, where it is largely removed in deep convective clouds.

To evaluate gaseous pollution sources with our model, we adopted the Emission Database for Global Atmospheric Research (EDGAR) (16). Table 2 indicates that the South and East Asian region is a substantial source of global pollution. For example, the total carbon monoxide (CO) release is estimated to be 50% larger than the combined emissions from Europe and North America. Table 2 also indicates that the nature of the pollution is different from that in Europe and North America. Particularly in India, the use of biofuels and agricultural burning causes substantial CO emissions.

Emissions from biomass burning are difficult to estimate because they usually occur scattered over large rural areas. Moreover, the burning process is not well defined because the fuel type and the combustion phase (flaming, smoldering) strongly affect the smoke composition (17). Many people in the Indian region still live in rural areas where

Fig. 1. Schematic overview of the INDOEX measurement domain, traversed by two ships (red hatching) and two aircraft (43 flights; yellow hatching), the mean location of the ITCZ, and 1- to 2-week boundary layer air mass trajectories during January to March 1999 (arrows). KCO is the Kaashidhoo Climate Observatory at 5°N , 73.5°E .

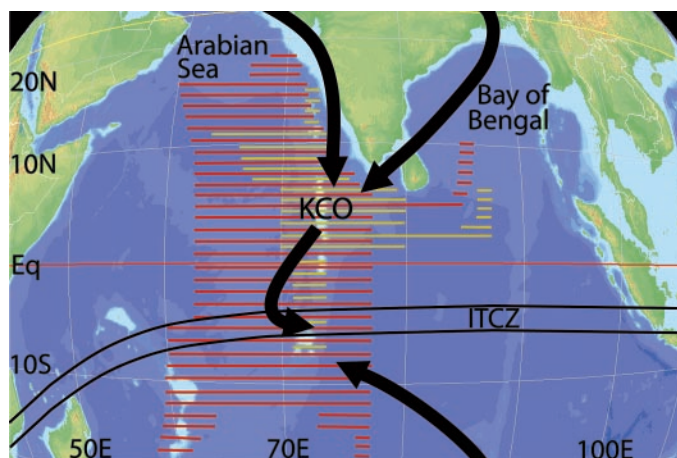


Fig. 2. Average mass (M) composition of fine aerosol on KCO (Maldives) as a function of the logarithm of the particle diameter (D) in February 1999. The residual includes mineral dust, fly ash, and unknown compounds (11).

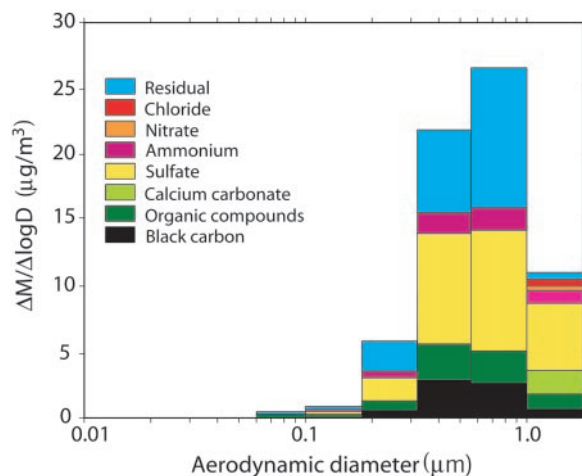


Table 1. Mean fine and coarse mass fractions of aerosols collected on filters on board the C-130 aircraft in the boundary layer (34 samples) and at KCO (24 samples). D is diameter. MSA is methane sulfonic acid. "Rest" includes magnesium, calcium, oxalate, formate, and unidentified material.

Compound	$D < 1 \mu\text{m}$ (%)	$D > 1 \mu\text{m}$ (%)
Sulfate	32	25
Organics	26	19
Black carbon	14	10
Mineral dust	10	11
Ammonium	8	11
Fly ash	5	6
Potassium	2	1
Nitrate	<1	4
Sea salt, MSA	<1	12
Rest	2	1
Total mass ($\mu\text{g}/\text{m}^3$)	22	17

REPORTS

domestic energy consumption largely depends on biofuels, whereas in urban areas, soft coke, kerosene, and other liquid fuels are also used. In Asia, about one-quarter of the energy use depends on biofuels, whereas in India, this fraction is larger, close to 50% (18, 19). It has been estimated that in India, firewood contributes about two-thirds to biofuel consumption, whereas the burning of dung and agricultural wastes contribute roughly equally to the remaining one-third (20–22).

A particularly useful indicator of biomass burning is the relative abundance of methyl cyanide (CH_3CN) to that of CO (23). The biomass burning emission of both gases mostly takes place from smoldering. The $\Delta\text{CH}_3\text{CN}/\Delta\text{CO}$ ratio measured on the C-130 aircraft and the R/V *Brown* was about 0.2% (Fig. 3) (24). This is close to the values obtained from controlled biomass fires in the laboratory (23). Without other substantial sources of CH_3CN , it follows that biomass burning was a major source of CO over the northern Indian Ocean. Measurements in air masses transported from southwestern Asia, mostly west of India (in blue), show a much lower $\Delta\text{CH}_3\text{CN}/\Delta\text{CO}$ ratio (Fig. 3), illustrating the importance of fossil fuel combustion as a pollution source to these air masses in addition to biomass burning (25). From our model simulations, which are in good agreement with the measurements, we infer that 60 to 90% of the CO originated from biomass burning (Fig. 4).

This model estimate is supported by a comparison of radiocarbon monoxide (^{14}CO) in low-latitude clean Southern Hemispheric air with that over the northern Indian Ocean, as measured from samples taken from the R/V *Brown*. The clean air samples south of the ITCZ contained on average 55 parts per billion by volume (ppbv) of CO and 6.2 molecules of $^{14}\text{CO}/\text{cm}^3$ whereas north of the ITCZ, this was 155 ppbv and 9.7 molecules/ cm^3 (26). The ^{14}CO difference between these air masses must be of biogenic origin, i.e., mainly biomass burning, because fossil fuels are radiocarbon-depleted. Previous analysis has shown that biomass burning adds 0.038 molecules of $^{14}\text{CO}/\text{cm}^3$ per ppbv of CO (26). If we assume further that about a third of the 55 ppbv of background CO is also related to biomass burning, as calculated with our model (Fig. 4B), it follows that the average contribution of biomass burning to CO over the northern Indian Ocean was 70 to 75%.

The highest pollution levels originated from the area around the Bay of Bengal (Table 3). The impact of these air masses over the Indian Ocean was largest in February. In March, the region was more strongly influenced by air that originated north of the Arabian Sea (Fig. 1). Although this air was generally cleaner, it also carried desert dust, which contributed to the aerosol load. The

aircraft measurements also show substantially enhanced methyl cyanide and methyl chloride (CH_3Cl) concentrations, particularly in air from the Bay of Bengal region. The latter points to the extensive use of chlorine-rich fuels such as agricultural waste and dung (27). Levels of NO only rarely exceeded the instrument detection limit of 40 parts per

trillion by volume (pptv) (only in fresh pollution plumes and downwind of ITCZ lightning), hence these are not shown.

We observed strongly enhanced CO levels over the northern Indian Ocean (28). Average CO mixing ratios at KCO in February were close to 200 ppbv. Such high CO concentrations are comparable to polluted air down-

Fig. 3. (A) Methyl cyanide (CH_3CN) versus carbon monoxide (CO) mixing ratios measured from the R/V *Brown* and calculated with a chemistry GCM. Average values are shown by the straight lines. The measurements (black) were performed between 12°S, 73°E and 17°N, 69°E. The measurements in blue represent air masses transported from the northwest, as determined by back-trajectory calculations (25). Because our chemistry GCM is unable to distinguish the air mass history, because it mixes the air masses at 1.8° resolution, the slope of the red line is less steep than of the black line.

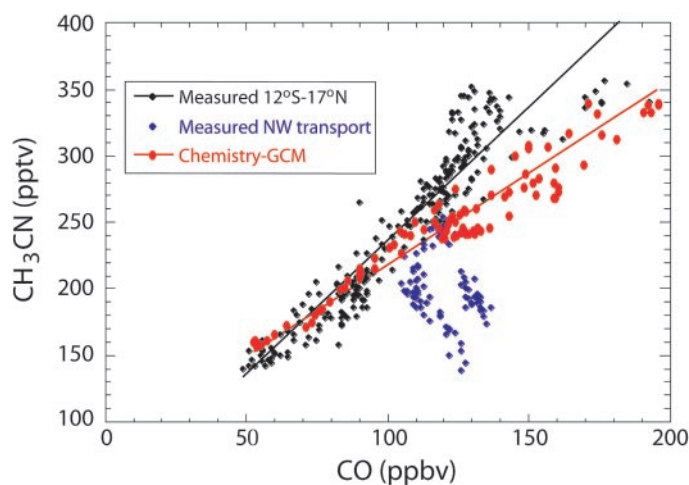


Table 2. Global anthropogenic CO_2 , CO, NO_x , SO_2 , and NMHC emissions (India region includes Bangladesh, Maldives, Sri Lanka, Myanmar, Nepal, and Pakistan. China region includes Cambodia, Vietnam, Laos, Mongolia, and North Korea. East Asia includes Japan, South Korea, Indonesia, Malaysia, Philippines, and Thailand) (16).

Source category	Global	North America	Europe	India	China	East Asia
<i>Carbon dioxide (Pg of CO_2 per year)</i>						
Total	29.8	6.2 (21%)	4.9 (16%)	2.2 (7%)	4.0 (13%)	2.5 (8%)
Fossil fuel use	21.9	5.6	4.5	0.7	2.6	1.7
Industrial processes	0.6	0.1	0.2	–	0.1	0.1
Biofuel use	5.5	0.5	0.2	1.4	1.2	0.5
Agriculture	1.8	–	–	0.1	0.1	0.2
<i>Carbon monoxide (Tg of CO per year)</i>						
Total	975	107 (11%)	85 (9%)	110 (11%)	111 (11%)	69 (7%)
Fossil fuel use	263	74	53	4	34	16
Industrial processes	35	2	8	1	5	6
Biofuel use	181	9	2	47	40	19
Agriculture	496	22	22	58	32	28
<i>Nitrogen oxides (Tg of NO_2 per year)</i>						
Total	102	26 (25%)	16 (16%)	6 (6%)	11 (10%)	6 (6%)
Fossil fuel use	72	24.3	13.6	2.6	7.2	4.3
Industrial processes	5	0.4	1.1	0.2	0.9	0.7
Biofuel use	5	0.5	0.2	1.1	1.5	0.4
Agriculture	20	0.8	0.7	2.0	1.1	1.0
<i>Sulfur dioxide (Tg of SO_2 per year)</i>						
Total	148	24.5 (17%)	33.3 (23%)	5 (3%)	28 (19%)	7 (5%)
Fossil fuel use	120	22.8	26.4	4.0	25.0	5.0
Industrial processes	23	1.2	6.4	0.3	2.8	1.7
Biofuel use	2	0.4	0.4	0.2	0.3	0.1
Agriculture	4	0.1	0.1	0.4	0.2	0.2
<i>Nonmethane hydrocarbons (Tg of NMHC per year)</i>						
Total	178	22 (12%)	21 (12%)	19 (11%)	17 (10%)	16 (9%)
Fossil fuel use	69	12	12	1.5	3	6
Industrial processes	34	7	7	3	4	4
Biofuel use	31	1	0.2	8.5	6	3
Agriculture	44	2	2	6	4	3

REPORTS

wind of North America and Europe. The KCO measurements show that aerosol absorption and scattering were highly correlated with CO, which indicates that the trace species of various origins were well mixed in the marine boundary layer (BL). Especially in February and early March, pollution levels at KCO varied strongly on a 3- to 7-day time scale. CO typically ranged from 120 to 250 ppbv. These changes were associated with tropical cyclones that transported cleaner air from the south (9). Later in March, the pollution levels near the surface were lower, largely associated with the air mass trajectory change from the northeast to the northwest. The aerosol optical thickness, however, was higher than in February. This indicates that particularly in March, substantial pollution transport took place above the BL.

Pollution variations over the northern Indian Ocean are also influenced by tropical waves that alter the intensity of ITCZ convection, acting on a 1- to 2-month time scale [known as the Madden Julian Oscillation (MJO)]. Strong convection ventilates the BL and increases the monsoonal flow (9). Furthermore, variations on an interannual time scale are affected by the El Niño–Southern Oscillation. During the recent El Niño in February 1998, for example, pollution transport from India was reduced, so that CO concentrations at KCO were only 110 to 140 ppbv. In February 1999, on the other hand, the monsoonal flow was strong, and hence pollution transport was efficient. In March 1999, the ITCZ convection intensified during an active phase of the MJO, which ventilated BL pollution from the Indian Ocean.

Considering that the pollution occurs at low latitudes, one expects strong photochemical activity, possibly giving rise to ozone (O_3) buildup. Because of its important role in atmospheric chemistry, O_3 was measured

from all platforms and ground stations, as well as through balloon soundings from KCO and the R/V *Brown* (29). In several O_3 profiles over KCO (Fig. 5A), sharp peaks can be discerned, with a particularly pronounced O_3 maximum above the BL. The O_3 minimum within the BL, which extended to an altitude of 0.5 to 1 km, and the maximum directly above are not well reproduced by the model. This is related to a sea breeze circulation at the Indian coast that is not resolved. During daytime, the convective BL over land extends to about 2 to 3 km, whereas further downwind, the marine BL only reaches about 1-km altitude or less (30, 31). The sea breeze causes upward transport over land that adds pollution to a stable layer that develops over the Indian Ocean between about 1 and 3 km in the monsoonal outflow from India. Because cumulus convection is weak in the Indian outflow, the layer can remain intact, which constitutes a “residual” pollution layer.

Typical altitude profiles of pollutants downwind of India, measured from the C-130 aircraft, also show the residual layer (Fig. 5B). In general, this layer was more pronounced in March than in February, related to

the growing convection over land as surface heating increases toward the end of winter. Some of the profiles also show a secondary maximum between 3- and 4-km altitude. Meteorological analysis indicates that these air masses were transported from the east, carrying pollution from Southeast Asia. On several occasions, it was observed that the vertical layering, shown in Fig. 5, can be maintained as far south as the Maldives, whereas further toward the ITCZ, trade wind cumulus convection causes breakup, vertical mixing, and partial dispersion into the free troposphere.

Although O_3 concentrations near the Indian coast were about 50 ppbv and peak values in the residual layer even reached 80 to 100 ppbv, photochemical destruction of O_3 prevents its accumulation over the Indian Ocean. Typically, O_3 decreased from ~50 ppbv at 15°N to ~10 ppbv near the ITCZ, which implies an O_3 loss rate in the BL of 1.5 to 2 ppbv per degree of latitude, or about 10%/day. Much pollution originates from biomass burning. In particular, smoldering fires produce relatively little NO_x , a necessary ingredient for photochemical O_3 formation ($NO_x = NO + NO_2$). Nevertheless,

Table 3. Mean results from boundary layer Citation aircraft measurements (25 flights) between the Maldives and the ITCZ during February to March 1999. The two main source regions of the measured air pollution have been determined by back-trajectory calculations (25) (standard deviations in parentheses).

	Source region	
	Bay of Bengal	Arabian Sea
CO (ppbv)	208 (42)	135 (16)
O_3 (ppbv)	15 (5)	13 (4)
$CH_3C(O)CH_3$ (ppbv)	2.2 (0.4)	1.6 (0.2)
CH_3CN (pptv)	288 (72)	266 (39)
C_2H_6 (pptv)	817 (251)	465 (134)
C_2H_2 (pptv)	291 (179)	81 (34)
C_3H_8 (pptv)	50 (36)	36 (41)
C_6H_6 (pptv)	99 (42)	40 (18)
CH_3Cl (pptv)	757 (64)	650 (30)

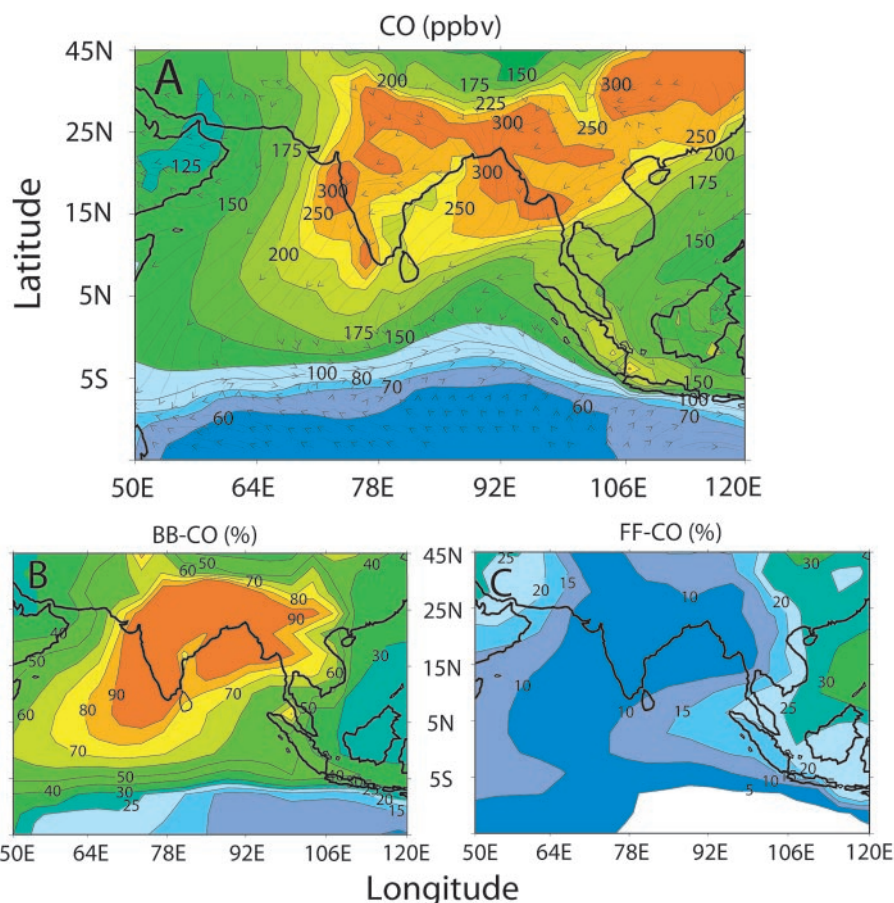


Fig. 4. (A) Mean CO (ppbv) near the surface over the Indian Ocean during February 1999, as calculated with our chemistry GCM (10). Average winds are shown by streamlines. Marked tracers indicate the percentage of CO from (B) biomass burning (BB)—mostly biofuel use and agricultural waste burning—and (C) fossil fuel (FF) combustion. The remainder largely originates from hydrocarbon oxidation.

REPORTS

several hundred pptv equivalent nitrate was measured in the coarse aerosols, which indicates that NO_x emissions are not negligible. However, NO_x is converted into nitrate by nighttime heterogeneous reactions on aerosols and daytime reaction with hydroxyl (OH) radicals, followed by uptake of HNO_3 by sea salt and dust particles. As a result, the NO_x lifetime is half a day or less, and its mixing ratio was generally quite low in the marine BL ($\text{NO} < 10$ pptv) (32), favoring chemical O_3 destruction rather than O_3 formation (33–36).

The combined anthropogenic NO_x source (S_N) from South and Southeast Asia is proportionally much smaller than the total CO and hydrocarbon source (S_C) as compared with Europe and North America. Thus, the ratio S_N/S_C (mol/mol) is comparatively low in Asia. The North American and European emissions, largely associated with high-temperature fossil fuel combustion, contain much more NO_x . This implies not only that O_3 photochemistry in the south-southeast Asian plume is strongly NO_x limited but also that OH regeneration by NO is inefficient (37, 38). On a global scale, OH regeneration by NO_x is about equally as important as the primary OH production by O_3 photodissociation (38). From our chemistry GCM, using the EDGAR emission database, we infer that the S_N/S_C ratio is more than four times lower in South and East Asia than in North America

and Europe. Our model calculations indeed indicate that human-produced emissions from South and East Asia reduce OH concentrations, whereas European and North American pollution has the opposite effect. Because OH is the foremost oxidant that removes natural and human-produced gases, the Asian pollution reduces the oxidizing power of the atmosphere. For example, it increases the lifetime of methane (CH_4), an important greenhouse gas.

Our results show that during the winter monsoon, South and Southeast Asian emissions cause considerable air quality degradation over an area in excess of 10 million km^2 . The nature of the pollution deviates from that in Europe and North America, a consequence of widespread biofuel use and agricultural burning, in support of the emission estimates in Table 2. In the next decades, emission trends in the region will likely reflect the additional use of fossil fuels, more strongly associated with NO_x emissions, boosting photochemical O_3 formation and the production of BC and sulfate, comparable to Europe and North America during the 1970s (39). However, considering the population size, the situation in Asia may become more serious. In southern Asia, the pollution buildup will be strongest in the winter monsoon under large-scale subsidence and cloud-free conditions. Unless international control mea-

asures are taken, air pollution in the Northern Hemisphere will continue to grow into a global plume across the developed and the developing world.

References and Notes

1. J. T. Houghton *et al.*, Eds., *Climate Change 1995: The Science of Climate Change* (Cambridge Univ. Press, Cambridge, 1996).
2. G. Marland *et al.*, *Global, Regional and National CO_2 Emissions* (Carbon Dioxide Information Analysis Center, Oak Ridge National Laboratory, Oak Ridge, TN, 1999) (available at <http://cdiac.esd.ornl.gov>).
3. S. Elliot *et al.*, *Geophys. Res. Lett.* **24**, 2671 (1997).
4. R. L. Arndt, G. R. Carmichael, D. G. Streets, N. Bhatti, *Atmos. Environ.* **31**, 1553 (1997).
5. W. L. Chameides *et al.*, *Geophys. Res. Lett.* **26**, 867 (1999).
6. D. O. Hall, F. Rosillo-Calle, J. Woods, *Chemosphere* **29**, 711 (1994).
7. J. Sathaye, S. Tyler, N. Goldman, *Energy* **19**, 573 (1994).
8. V. Ramanathan *et al.*, *Indian Ocean Experiment (INDOEX)* (C⁴ publication #162, University of California, San Diego, CA, 1996) (available at <http://www.c4-ucsd.edu>).
9. T. N. Krishnamurti, B. Jha, P. J. Rasch, V. Ramanathan, *Meteorol. Atmos. Phys.* **64**, 123 (1997). For a review of the monsoon meteorology and the role of El Niño, see P. J. Webster *et al.*, *J. Geophys. Res.* **103**, 14451 (1998).
10. Computer simulations with an interactive chemistry GCM have been performed at T63 resolution (1.8° latitude and longitude). The chemistry GCM has been described by G. J. Roelofs and J. Lelieveld [*Tellus* **49B**, 38 (1997)] and E. Roegner *et al.* [*J. Clim.* **12**, 3004 (1999)]. To represent actual meteorology, we assimilated analyses from the European Centre for Medium-Range Weather Forecasts (ECMWF), as described by A. T. J. de Laat *et al.* (35). The T63 resolution model version has been evaluated by A. S. Kentarchos, G. J. Roelofs, and J. Lelieveld [*J. Atmos. Sci.* **57**, 2824 (2000)]. The chemistry scheme includes a representation of higher hydrocarbons as described by G. J. Roelofs and J. Lelieveld [*J. Geophys. Res.* **105**, 22697 (2000)].
11. Aerosol sampling, as used at KCO, the R/V *Brown*, and the C-130 aircraft, and associated chemical analysis techniques are described by C. Leck and C. Persson [*Tellus* **48B**, 272 (1996)]; T. Novakov, D. A. Hegg, and P. V. Hobbs [*J. Geophys. Res.* **102**, 30023 (1997)]; L. S. Hughes *et al.* [*Environ. Sci. Technol.* **32**, 1153 (1998)]; M. O. Andreae *et al.* [*Tellus* **52B**, 1066 (2000)]; and H. Maring *et al.* [*J. Geophys. Res.* **105**, 14677 (2000)]. Single-particle analysis was performed by aerosol time-of-flight spectrometry, as described by P. J. Silva and K. A. Prather [*Environ. Sci. Technol.* **31**, 3074 (1997)] and E. E. Gard *et al.* [*Science* **279**, 1184 (1998)]. Aerosol measurements on the Citation aircraft were performed according to F. Schröder and J. Ström [*Atmos. Res.* **44**, 333 (1997)]. On KCO and the C-130 aircraft, aerosol optical properties were measured according to T. L. Anderson *et al.* [*J. Geophys. Res.* **104**, 26793 (1999)] and P. J. Sheridan and J. A. Ogren [*J. Geophys. Res.* **104**, 16793 (1999)]. At KCO, four cascade impactors were operated simultaneously, each with six stages (size ranges). The number of cascade impactor substrates analyzed, resulting in Fig. 2, was 192.
12. According to a review by J. Heintzenberg [*Tellus* **41B**, 149 (1989)], in North America and Europe, urban fine aerosols typically contain 28% sulfate, 31% organics, 9% BC, 8% ammonium, 6% nitrate, and 18% other material (mean mass = 32 $\mu\text{g}/\text{m}^3$); suburban aerosols contain 37% sulfate, 24% organics, 5% BC, 11% ammonium, 4% nitrate, and 19% other material (mean mass = 15 $\mu\text{g}/\text{m}^3$); and remote continental aerosols contain 22% sulfate, 11% organics, 3% BC, 7% ammonium, 3% nitrate, and 56% other material (mean mass = 4.8 $\mu\text{g}/\text{m}^3$). Additional data on different aerosol types, consistent with this review, are presented by J. H. Seinfeld and S. N. Pandis [*Atmospheric Chemistry and Physics* (Wiley, New York, 1998)].

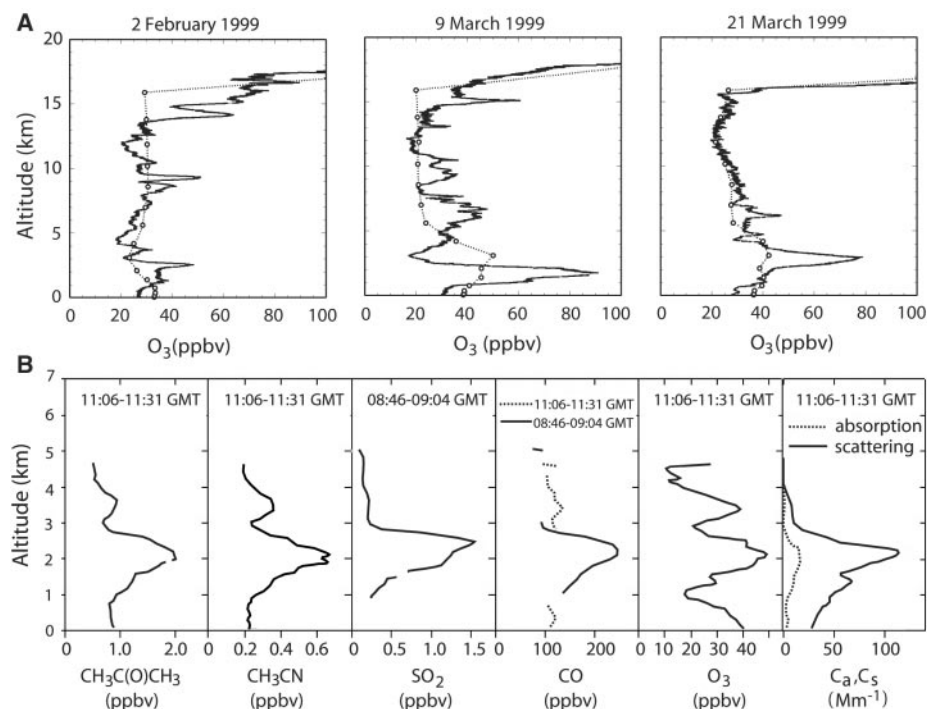


Fig. 5. (A) Ozone profiles over KCO as measured from balloon sondes and calculated with a chemistry GCM (dashed lines). The soundings show instances where the pronounced layering of the lower troposphere has remained intact as far south as 5°N. (B) Pollutant profiles downwind of India (7.5°N, 72°E), including aerosol absorption and scattering, observed from the C-130 aircraft on 13 March 1999.

13. A. S. Ackerman *et al.*, *Science* **288**, 1042 (2000).
14. S. K. Satheesh, V. Ramanathan, *Nature* **405**, 60 (2000); V. Ramanathan, unpublished data.
15. W. F. Cooke *et al.*, *J. Geophys. Res.* **104**, 22137 (1999). The BC/total carbon and organic carbon/BC ratios observed during INDOEX much resemble those in urban Japan and Korea [T. Novakov *et al.*, *Geophys. Res. Lett.* **27**, 4061 (2000)]. These ratios were nearly constant over the Indian Ocean, whereas total carbon and BC were highly correlated ($r^2 = 0.81$), providing strong indications of the primary nature of the INDOEX aerosol carbon.
16. J. G. J. Olivier *et al.*, *Description of EDGAR Version 2* (RIVM Report 771060002, National Institute for Public Health and Environment, Bilthoven, Netherlands, 1996) [available at <http://www.rivm.nl>]. An update is presented by J. A. van Aardenne *et al.* (*Global Biogeochem. Cycles*, in press). The EDGAR estimates of Asian CO emissions from biofuel combustion are about 20% lower compared with the inventory by D. G. Streets and S. T. Waldhoff [*Energy* **24**, 841 (1999)].
17. P. J. Crutzen, M. O. Andreae, *Science* **250**, 1669 (1990).
18. L. Srivastava, *Energy Policy* **25**, 941 (1997).
19. D. G. Streets, S. T. Waldhoff, *Energy* **23**, 1029 (1998).
20. N. H. Ravindranath, J. Ramakrishna, *Energy Policy* **25**, 63 (1997).
21. C. S. Sinha, S. Sinha, V. Joshi, *Biomass Bioenergy* **14**, 489 (1998).
22. A. K. Mahapartra, C. P. Mitchell, *Biomass Bioenergy* **17**, 291 (1999).
23. The $\Delta\text{CH}_3\text{CN}/\Delta\text{CO}$ molar ratio refers to the enhancement of these gases compared with background air. The lowest concentrations of CH_3CN (140 pptv) and CO (50 ppbv), observed south of the ITCZ, have been used as background values (pptv is parts per trillion by volume or pmol/mol; ppbv is parts per billion by volume or nmol/mol). $\text{CH}_3\text{CN}/\text{CO}$ from biomass burning varies according to the fuel type and the burning temperature. The measurements by J. M. Lobert *et al.* [in *Global Biomass Burning: Atmospheric, Climatic and Biospheric Implications*, J. S. Levine, Ed. (MIT Press, Cambridge, MA, 1991), pp. 289–304] and by R. Holzinger *et al.* [*Geophys. Res. Lett.* **26**, 1161 (1999)] indicate a mean range of 0.13 to 0.25%.
24. The instrumentation on board the Citation aircraft has been described by J. Lelieveld *et al.* [*J. Geophys. Res.* **104**, 8201 (1999)]. On the Citation, C-130 aircraft, and the R/V *Brown*, CH_3CN and $\text{CH}_3\text{C}(\text{O})\text{CH}_3$ have been measured by proton-transfer-reaction mass spectrometry, as described by W. Lindinger, A. Hansel, and A. Jordan [*Int. J. Mass Spectrom Ion Proc.* **173**, 191 (1998)]. On the C-130 aircraft, these gases and SO_2 were also measured by chemical ionization mass spectrometry. On the Citation aircraft, CO was measured by tunable diode laser spectrometry (TDLAS), as described by F. G. Wienhold *et al.* [*Appl. Phys.* **B67**, 411 (1998)]; on the R/V *Brown*, CO was measured by TDAS, as described by H. Fischer *et al.* [*J. Geophys. Res.* **102**, 23559 (1997)].
25. The source analysis of measured pollution has been supported by back-trajectory calculations. The trajectory model uses high-resolution ECMWF-analyzed meteorological data, as described by M. P. Scheele, P. C. Siegmund, and P. F. J. van Velthoven [*Meteorol. Appl.* **3**, 267 (1996)].
26. The measurements refer to nine 600-liter canister samples, three collected south and six north of the ITCZ, analyzed according to the method of C. A. M. Brenninkmeijer [C. A. M. Brenninkmeijer, *J. Geophys. Res.* **98**, 10595 (1993); C. A. M. Brenninkmeijer *et al.*, *Chemosphere Global. Change Sci.* **1**, 33 (1999)]. ^{14}C can result from biomass burning and the oxidation of natural hydrocarbons. Forest emissions of hydrocarbons, however, are small, whereas hydrocarbon oxidation is minimal during winter.
27. We observed a mean molar enhancement of CH_3Cl relative to CO of 1.98×10^{-3} in the marine BL, a strong indication of biomass burning emissions; see W. C. Keene *et al.*, *J. Geophys. Res.* **104**, 8429 (1999); J. M. Lobert *et al.*, *J. Geophys. Res.* **104**, 8373 (1999). We found high correlations ($r^2 = 0.9$) of CH_3Cl with CO, CH_3CN , C_2H_2 , and C_6H_6 , all products from incomplete (biomass) combustion.
28. On the R/V *Brown* and on the C-130 aircraft, CO was measured according to R. R. Dickerson and A. C. Delany [*J. Atmos. Oceanic Technol.* **5**, 424 (1988)]; on KCO, CO was measured according to M. Cogan and J. M. Lobert [*Proceedings of the 43rd Annual ISA Analysis Division Symposium*, vol. 31 (Instrument Society of America, Research Triangle Park, NC, 1998), pp. 229–234. See also (24)].
29. Ozone measurements were performed from balloons with Electrochemical Concentration Cell sondes coupled to Väisälä radiosondes, on KCO as described by W. D. Komhyr *et al.* [*J. Geophys. Res.* **100**, 9231 (1995)], and on the R/V *Brown* as described by D. Kley *et al.* [*Q. J. R. Met. Soc.* **123**, 2009 (1997)].
30. M. Venkata Ramana *et al.*, *Curr. Sci.* **76**, 931 (1999).
31. O. P. Madan *et al.*, *Meteorological Analysis During INDOEX Intensive Field Phase—1999* (Centre for Atmospheric Sciences, New Delhi, India, 1999).
32. NO, as measured from the Citation aircraft, was generally below the detection limit of 40 pptv. On the R/V *Brown*, NO was generally below 10 pptv (T. P. Carsey, R. R. Dickerson, M. L. Farmer, unpublished data).
33. K. P. Rhoads *et al.*, *J. Geophys. Res.* **102**, 18981 (1997).
34. S. Lal, M. Naja, A. Jayaraman, *J. Geophys. Res.* **103**, 18907 (1998).
35. A. T. J. de Laat *et al.*, *J. Geophys. Res.* **104**, 13881 (1999).
36. M. Naja *et al.*, *Curr. Sci.* **76**, 931 (1999).
37. Y. Wang, D. J. Jacob, *J. Geophys. Res.* **103**, 31123 (1998).
38. P. J. Crutzen, M. G. Lawrence, U. Pöschl, *Tellus* **51AB**, 123 (1999). Primary OH production occurs through O_3 photodissociation by solar shortwave radiation in the presence of water vapor [the reaction $\text{O}(^1\text{D}) + \text{H}_2\text{O} \rightarrow 2\text{OH}$]. After the initial loss of OH through its reaction with a pollutant gas, e.g., CO, a peroxy radical (e.g., HO_2) is formed, which can react with NO , yielding NO_2 and regenerating OH. NO_2 subsequently photodissociates and forms O_3 .
39. The Asian emissions of CO, nonmethane hydrocarbons (NMHC), NO_x , and SO_2 will strongly depend on the fuel mix used (coal, oil, and biofuels) and the efficiency of industrial and traffic emissions. Two-stroke engines, for example, which are widely used in India, burn at relatively low temperatures so that NO_x emissions are limited and CO and NMHC emissions are large. The Intergovernmental Panel on Climate Change [*Emission Scenarios* (Cambridge Univ. Press, Cambridge, 2000)] estimates that CO_2 , CO, NO_x , SO_2 , and NMHC emissions in Organization for Economic Cooperation and Development countries will change from 2000 to 2020 by 2 to 24%, –14 to 27%, –13 to 30%, –60 to –49%, and –8 to 5%, respectively (hence partly reductions), whereas in Asia, these emissions will grow by 41 to 104%, 7 to 34%, 50 to 81%, 15 to 114%, and 9 to 89%, respectively.
40. We are grateful for the support by many funding agencies, notably the NSF, the Department of Energy, NASA, the National Oceanic and Atmospheric Administration, the Indian Space Research Organization, the European Union, the Max-Planck-Gesellschaft, the French Centre National d'Etudes Spatiales, the Netherlands Supercomputing Facility, and the Netherlands Organization for Scientific Research. We thank J. Olivier for his help with emission estimates (16, 39).

2 November 2000; accepted 10 January 2001

Recolonizing Carnivores and Naïve Prey: Conservation Lessons from Pleistocene Extinctions

Joel Berger,^{1*} Jon E. Swenson,² Inga-Lill Persson^{3†}

The current extinction of many of Earth's large terrestrial carnivores has left some extant prey species lacking knowledge about contemporary predators, a situation roughly parallel to that 10,000 to 50,000 years ago, when naïve animals first encountered colonizing human hunters. Along present-day carnivore recolonization fronts, brown (also called grizzly) bears killed predator-naïve adult moose at disproportionately high rates in Scandinavia, and moose mothers who lost juveniles to recolonizing wolves in North America's Yellowstone region developed hypersensitivity to wolf howls. Although prey that had been unfamiliar with dangerous predators for as few as 50 to 130 years were highly vulnerable to initial encounters, behavioral adjustments to reduce predation transpired within a single generation. The fact that at least one prey species quickly learns to be wary of restored carnivores should negate fears about localized prey extinction.

The spectacular post-Pleistocene extinctions of many genera of large animals in areas ranging from Australia to North America have been attributed primarily to human overkill as hunters encountered naïve prey—the “blitzkrieg hypothesis” (1)—and/or to climate change (2). An inadvertent consequence of today's extinction of many large carnivores is that prey in otherwise intact areas may lose knowledge about current predators (3, 4). These extinctions, however, offer op-

portunities to assess the generality of components of the blitzkrieg hypothesis and to address concerns about the ecological consequences of carnivore restoration. In Western Europe and the United States (outside of Alaska), wolves (*Canis lupus*) and brown bears (*Ursus arctos*) were eliminated within 100 years from more than 95% of their range. The cessation of predation has released mammalian prey from past selection pressures (3–5), but the current expansion of large car-